CMS Physics Analysis Summary

Contact: cms-pag-conveners-susy@cern.ch 2019/08/03

Search for supersymmetry with a compressed mass spectrum in events with a soft τ lepton, a highly energetic jet, and large missing transverse momentum in proton-proton collisions at $\sqrt{s} = 13$ TeV

The CMS Collaboration

Abstract

The first search for supersymmetry in events with one soft tau lepton, one energetic jet from initial state radiation, and transverse momentum imbalance is presented. These event signatures are consistent with those from supersymmetric models exhibiting co-annihilation between the scalar tau lepton ($\tilde{\tau}$) and the lightest neutralino ($\tilde{\chi}_1^0$) that could generate the observed relic density of dark matter. The data correspond to an integrated luminosity of 77.2 fb^{-1} of proton-proton collisions at $\sqrt{s} = 13$ TeV collected with the CMS detector at the CERN LHC in 2016 and 2017. The results are interpreted considering a supersymmetric scenario with a small mass difference (Δm) between the chargino ($\tilde{\chi}_1^{\pm}$) or the next-to-lightest neutralino ($\tilde{\chi}_2^0$), and the lightest neutralino. The mass of the $\tilde{\tau}$ is defined as the average of the $\tilde{\chi}_1^{\pm}/\tilde{\chi}_2^0$ and $\tilde{\chi}_1^0$ masses. The data are found to be consistent with the standard model background predictions. Upper limits at 95% confidence level are set on the $\tilde{\chi}_1^{\pm}$, $\tilde{\chi}_2^0$, and $\tilde{\tau}$ production cross sections for $\Delta m(\tilde{\chi}_1^{\pm}, \tilde{\chi}_1^0) = 50$ GeV, resulting in a lower mass limit of 290 GeV on the mass of the $\tilde{\chi}_1^{\pm}/\tilde{\chi}_2^0$, which is the most stringent to date.

Supersymmetry (SUSY) [1–7] is an extension of the standard model (SM) that could describe the particle nature of dark matter (DM) and potentially solve the gauge hierarchy problem. In SUSY models assuming $\mathcal{R}$-parity [8] conservation, the lightest neutralino ($\widetilde{\chi}_1^0$), as the lightest supersymmetric particle (LSP), is neutral, stable, and could have undergone the right amount of annihilation-production interactions with SM particles in the early universe to give rise to the DM relic density observed today [9, 10]. However, in SUSY models with a bino LSP, these interactions alone are not sufficient to produce the correct DM relic abundance. In these cases, a model of co-annihilation (CA) can be introduced [11].

This letter describes a search for the production of stau particles ($\widetilde{\tau}$), the SUSY partners of the tau (τ) lepton, considering scenarios where the mass difference between the $\widetilde{\chi}_1^0$ and the $\widetilde{\tau}$, Δm, is small. This is motivated by models considering $\widetilde{\tau} - \widetilde{\chi}_1^0$ CA [11–18], where the calculated relic DM density is consistent with the one measured by the WMAP and Planck Collaborations [9, 10]. The small mass difference enhances the $\widetilde{\tau} - \widetilde{\chi}_1^0$ CA cross-section due to its dependence on $e^{-\Delta m}$, thereby driving down the predicted DM relic density to a value consistent with experimental measurements.

In proton-proton (pp) collisions at the LHC, $\widetilde{\tau}$ particles can be produced either directly in pairs ($\mathrm{pp} \to \widetilde{\tau}\widetilde{\tau}$) or in decays of heavier SUSY particles. The $\widetilde{\tau}$ subsequently decays to a τ lepton and $\widetilde{\chi}_1^0$. This analysis requires an extra jet (j) from initial state radiation (ISR). Therefore, this analysis focuses on $\mathrm{pp} \to \tilde{\tau}\tilde{\tau}\mathrm{j}$ production and indirect $\tilde{\tau}$ production via decays of the lightest chargino, $\widetilde{\chi}_1^\pm$, or the next-to-lightest neutralino, $\widetilde{\chi}_2^0$, in processes such as $\mathrm{pp} \to \widetilde{\chi}_1^\pm\widetilde{\chi}_1^\mp\mathrm{j} \to \widetilde{\tau}\widetilde{\tau}\nu_\tau\nu_\tau\mathrm{j} \to \tau\widetilde{\chi}_1^0\tau\widetilde{\chi}_1^0\nu_\tau\nu_\tau\mathrm{j}$, $\mathrm{pp} \to \tilde{\chi}_1^\pm\tilde{\chi}_2^0\mathrm{j} \to \widetilde{\tau}\nu_\tau\widetilde{\tau}\tau\mathrm{j} \to \tau\widetilde{\chi}_1^0\tau\tau\widetilde{\chi}_1^0\tau\mathrm{j}$, and $\mathrm{pp} \to \tilde{\chi}_2^0\tilde{\chi}_2^0\mathrm{j} \to \widetilde{\tau}\tau\widetilde{\tau}\tau\mathrm{j} \to \tau\widetilde{\chi}_1^0\tau\tau\widetilde{\chi}_1^0\tau\mathrm{j}$. The recoil effect (kinematic boost) created by the ISR jet facilitates both detection of transverse momentum imbalance ($p_\mathrm{T}^\mathrm{miss}$) and identification of the soft τ lepton decay products [19]. While the above processes result in final states with multiple τ leptons, the small Δm constrains the transverse momentum (p_T) of the τ leptons to $\approx \Delta m/2$, which is further reduced after the decays of τ leptons. Therefore, for small Δm scenarios, it is difficult to reconstruct and identify multiple τ leptons. Furthermore, semi-leptonic decays of τ leptons result in lower average p_T than hadronic decays (τ_h), while also being largely indistinguishable from prompt production of electrons and muons. In addition, τ_h final states have the largest branching fraction, around 64%, of all tau decays. For these reasons, we search for events with exactly one low-energy (soft) τ_h candidate recoiling against a high-p_T ISR jet.

The search strategy outlined above allows this analysis to probe the $\widetilde{\tau}$-$\widetilde{\chi}_1^0$ CA region with $\Delta m(\widetilde{\chi}_1^0, \widetilde{\tau}) < 50\,\mathrm{GeV}$. This is the first collider search for compressed SUSY using this search strategy. Searches in the CA region perfomed by CMS [20, 21] and ATLAS [22, 23], using different strategies, have not surpassed the results from the LEP experiments [24–27]. The analysis is performed using data collected in 2016 and 2017 with the CMS experiment [28] at the LHC in pp collisions at a center-of-mass energy ($\sqrt{s}$) of 13 TeV. The data sample corresponds to an integrated luminosity of $77.2\,\mathrm{fb}^{-1}$.

The central feature of the CMS apparatus [28] is a superconducting solenoid of 6 m internal diameter, providing a magnetic field of 3.8 T. Within the solenoid volume are a silicon pixel and strip tracker, a lead tungstate crystal electromagnetic calorimeter (ECAL), and a brass and scintillator hadron calorimeter, each composed of a barrel and two endcap sections. Forward calorimeters extend the pseudorapidity (η) coverage provided by the barrel and endcap detectors up to $|\eta| < 5.2$. Muons are measured in gas-ionization detectors embedded in the steel flux-return yoke outside the solenoid. A more detailed description of the CMS detector can be found in Ref. [28].

Events are reconstructed from particle candidates (electrons, muons, photons, and charged

and neutral hadrons) identified using the particle-flow (PF) algorithm [29]. The PF algorithm combines information from all detectors to classify final-state particles produced in the pp collision. The anti-k_T clustering algorithm [30] with a distance parameter of 0.4 is used to reconstruct jets. Identification criteria are applied to jet candidates to remove anomalous effects from the calorimeters. For jets with $p_T > 30\,\text{GeV}$ and $|\eta| < 2.4$ the identification efficiency is >99% [31].

In simulation the jet energy scale and resolution are corrected using scale factors, that depend on the p_T and η of the jet, to match the values measured in data [32]. Jets originating from the hadronization of bottom quarks are identified using the combined secondary vertex algorithm [33]. This analysis uses the loose working point of the algorithm, which has an identification efficiency of 80% and a light flavor quark or gluon misidentification rate of 10%.

Electrons are reconstructed and identified combining information from the ECAL and the tracking systems [34]. Muons are reconstructed using the tracker and muon chambers. A track in the central tracker is required to be consistent with measurements in the muon chambers and low energy measurements in the calorimeters [35]. For this analysis the muon (electron) identification efficiency is 96% (85%), for muons (electrons) with $p_T > 10\,\text{GeV}$ and $|\eta| < 2.1$.

Hadronic decays of the τ leptons are reconstructed and identified using the hadrons-plus-strips algorithm [36], designed to optimize the performance of τ_h reconstruction by considering specific τ_h decay modes. To suppress backgrounds from light flavor quark or gluon jets, identification and isolation conditions are enforced by requiring the τ_h candidates to pass a threshold value of a multivariate (MVA) discriminator [36] that takes isolation variables and variables related to the τ lepton lifetime as input. The "tight" MVA isolation working point [36] is used, which results in a τ_h identification efficiency of typically 55% for the kinematic range used in this analysis. The τ_h candidates are also required to be distinguishable from electrons and muons.

The value of p_T^{miss} is the magnitude of the negative vector sum of the transverse momenta of all PF candidates. The prevailing SM background processes contributing to the search are W+jets and Z+jets events (where the bosons decay to τ leptons), top quark pairs ($t\bar{t}$), and quantum chromodynamics (QCD) multijet processes. The contributions of W +jets and Z+jets events contain genuine, well-isolated τ_h candidates, energetic jets, and true p_T^{miss} from associated neutrinos present in the τ lepton and W decays. Background from $t\bar{t}$ events is characterized by two b quark jets in addition to genuine isolated τ_h leptons. The QCD multijet events are characterized by jets with a high-multiplicity of particles which can be misidentified as τ_h.

To estimate the background contributions, a combination of Monte Carlo (MC) simulated samples and techniques based on data are employed. Simulated samples for Z+jets, W+jets, $t\bar{t}$+jets, and single-top quark events are produced with the MADGRAPH5_aMC@NLO 2.6.0 program [37] at leading order (LO) precision. The MADGRAPH5_aMC@NLO generator is interfaced with PYTHIA8.212 [38] using the CUETP8M1 tune [39], for parton shower and fragmentation. The LO PYTHIA generator is used to model the diboson (VV) processes. The simulation of the CMS detector is performed using the GEANT4 [40] package. Simulated events are corrected to account for the effects of additional pp interactions present in data.

Two sets of signal event samples are generated using the MADGRAPH5_aMC@NLO v.2.3.3 generator at LO precision. The simulation of the detector is performed using the CMS fast simulation package [41]. Systematic uncertainty is included in the exclusion limits to account for differences between the fast and GEANT4 simulation. The first set of signal samples considers pair production of $\tilde{\chi}_1^{\pm}$ and $\tilde{\chi}_2^0$ gauginos ($\tilde{\chi}_1^{\pm}\tilde{\chi}_1^{\mp}$ and $\tilde{\chi}_1^{\pm}\tilde{\chi}_2^0$) with up to two associated jets. Models

with a bino $\widetilde{\chi}_1^0$ and wino $\widetilde{\chi}_2^0$ and $\widetilde{\chi}_1^\pm$ are considered. For interpretations of our results we assume a left-handed $\widetilde{\tau}$ and that $Br(\widetilde{\chi}_2^0 \to \tau\widetilde{\tau} \to \tau\tau\widetilde{\chi}_1^0) = 100\%$ and $Br(\widetilde{\chi}_1^\pm \to \nu\widetilde{\tau} \to \nu\tau\widetilde{\chi}_1^0) = 100\%$. Also, the mass of the $\widetilde{\chi}_1^\pm$ and $\widetilde{\chi}_2^0$ are considered to be equal. We will henceforth refer to this model as SUSY Signal Model 1 (SSM1). The second set considers the direct production of left-handed $\widetilde{\tau}$ pairs with up to two associated jets. We will henceforth refer to this model as SUSY Signal Model 2 (SSM2). The MC background yields are normalized to the integrated luminosity using next-to-next-to-leading (NNLO) order or next-to-leading order (NLO) cross sections, while the signal production cross sections are calculated at NLO with next-to-leading logarithmic (NLL) soft-gluon resummation calculations [42–45].

Events are initially preselected using a $p_{\mathrm{T}}^{\mathrm{miss}}$-based trigger that does not have any τ_{h} requirements. The trigger efficiency as function of $p_{\mathrm{T}}^{\mathrm{miss}}$ is measured using data events in which one muon is reconstructed, which results in a control sample that is 95% pure W+jets events. The efficiency reaches a plateau of 100% at around 200 GeV. Selected signal events are required to have $p_{\mathrm{T}}^{\mathrm{miss}} > 230\,\mathrm{GeV}$ such that the trigger is fully efficient for these events. Events are also required to have exactly one identified τ_{h} candidate, reconstructed within the pseudorapidity region of $|\eta| < 2.1$. The p_{T} of the τ_{h} candidate is bounded to $20\,\mathrm{GeV} < p_{\mathrm{T}}(\tau_{\mathrm{h}}) < 40\,\mathrm{GeV}$. The upper limit on the transverse momentum allows considerable reduction of the W+jets, Z+jets, and $\mathrm{t\bar{t}}$+jets background contributions to the search region. Events are also required to have at least one jet with $p_{\mathrm{T}} > 30\,\mathrm{GeV}$ and $|\eta| < 2.4$. The jet with the highest p_{T} is referred to as the ISR jet and is required to satisfy $p_{\mathrm{T}} > 100\,\mathrm{GeV}$. The absolute difference in the azimuthal angle, ϕ, between the ISR jet and the $p_{\mathrm{T}}^{\mathrm{miss}}$ is used to reduce the contribution from QCD multijet events ($|\Delta\phi(\mathrm{j}_{lead}, p_{\mathrm{T}}^{\mathrm{miss}})| > 0.7$). To reduce background processes with top quarks, such as single top and $\mathrm{t\bar{t}}$, events with jets tagged as b quarks are rejected. Finally, events with well identified and isolated electrons or muons (p_{T} (e), p_{T} (μ) $> 10\,\mathrm{GeV}$) are also rejected.

The transverse mass between the selected τ_{h} candidate and the $p_{\mathrm{T}}^{\mathrm{miss}}$, defined as

$$m_{\mathrm{T}}(p_{\mathrm{T}}^{\mathrm{miss}}, \tau_{\mathrm{h}}) = \sqrt{2p_{\mathrm{T}}^{\mathrm{miss}} p_{\mathrm{T}}(\tau_{\mathrm{h}})(1 - \cos\Delta\phi(p_{\mathrm{T}}^{\mathrm{miss}}, \tau_{\mathrm{h}}))},$$

is used as the main observable to search for the presence of signal events.

The dominant backgrounds are estimated from data, using control regions (CR) enriched in the targeted background processes and with negligible contamination from signal events. MC simulations are used to extrapolate dominant background yields from a CR to the signal region (SR) and to model the shape of subdominant background contributions. The level of agreement between data and MC in these CRs allows us to validate the correct modeling of the τ_{h} selections and to measure data-to-simulation scale factors to correct the modeling of the ISR jet and the $p_{\mathrm{T}}^{\mathrm{miss}}$. To calculate the correction factor for a background process, the contribution from all other backgrounds is subtracted from the data. The uncertainty on the other background processes is propagated to the final systematic uncertainty on the background predictions. The contribution from small backgrounds, such as single top and diboson production, is estimated using simulation.

The correct modeling in the simulation of background events can be affected by the requirement of an ISR jet in the event topology. This modeling is studied using a $\mathrm{Z}(\to \mu\mu)$+jets control region in data. The use of $\mathrm{Z}(\to \mu\mu)$+jets provides a direct measurement of the p_{T} spectrum resulting from the radiation of a high-p_{T} ISR jet, decoupling the effects of ISR modeling from the measurement of $p_{\mathrm{T}}^{\mathrm{miss}}$. The p_{T} of the Z boson ($p_{\mathrm{T}}(\mu\mu)$) is measured by vectorially summing the transverse momenta of the two muons from the Z decay. The ratio between data and simulation in the $p_{\mathrm{T}}(\mu\mu)$ distribution is used to obtain p_{T}-dependent correction factors, which range from 0.79 to 1.12, that are subsequently applied to each event in simulation satisfying the event

selection criteria. The correction factors are validated using a $W(\rightarrow \mu\nu_{\mu})$+jet enriched sample. After applying the correction factors in the $W(\rightarrow \mu\nu_{\mu})$+jets enriched sample, agreement is observed (within the statistical and systematic uncertainties) between the observed and predicted yields and shapes of distributions. It is noted these ISR correction factors are applied to all Drell-Yan processes, including the simulated signal processes involving virtual W and Z bosons.

A $Z(\rightarrow \tau_h\tau_h)$+jets CR is defined to study the modeling of τ_h reconstruction and identification. The CR is obtained by requiring two well identified τ_h candidates with $p_T > 60\,\text{GeV}$ and $|\eta| < 2.1$, selected by a dedicated $\tau_h\tau_h$ trigger. The τ_h pair must have opposite electric charge and a reconstructed mass between 50 and 100 GeV, and all other requirements are the same as for SR events. The contribution of QCD multijet events in the $Z(\rightarrow \tau_h\tau_h)$+jets CR is estimated from data using CRs obtained with τ_h pairs with the same electric charge. The transfer factor between same and opposite-sign events is calculated using events with loosened τ_h isolation requirements and $m(\tau_h\tau_h) > 100\,\text{GeV}$. A correction factor of 0.92 ± 0.05 (0.95 ± 0.04) for $Z(\rightarrow \tau_h\tau_h)$+jets is measured in this CR for the 2016 (2017) data set. The quoted uncertainties are purely statistical. These correction factors, which account for mismodeling of the overall selection efficiencies in simulation, are used to scale the $Z(\rightarrow \tau\tau)$+jets prediction in the SR.

The contribution from $t\bar{t}$ events in the SR is less than 15% of the total expected background. A correction factor of 0.94 ± 0.05 (0.95 ± 0.04) is measured for the 2016 (2017) data set in a CR obtained by selecting events with two b-tagged jets and one τ_h candidate with tighter isolation requirements with respect to the SR. These requirements allow for a $t\bar{t}$ CR sample with high purity. The correction factor derived from the CR is applied to scale the prediction of $t\bar{t}$ events in the SR.

To determine the contribution from QCD multijet events in the SR, a fully data-driven method is used. A CR enriched with QCD multijet events (CR_{QCD}) is obtained by requiring the same criteria for the SR but τ_h selecting candidates that fail the tight but pass the loose τ_h isolation. The contribution from non-multijet events are subtracted using simulation, adjusted for the scale factors discussed above. The shape and normalization of the multijet background is predicted by multiplying the data yields in CR_{QCD} with transfer factors (or "tight-to-loose" ratios) to account for the isolation efficiency. The $p_T(\tau_h)$-dependent transfer factors are derived in a $W(\rightarrow \mu\nu)+\tau_h$ CR, where the τ_h is in reality a misidentified jet. These transfer factors are validated in a region enriched in QCD multijet events by inverting the $\Delta\phi(j_{lead}, p_T^{miss})$ requirement.

One main source of systematic uncertainty arises from the τ_h identification and isolation requirements, which amount to between 6% and 9% depending on the SM background and signal sample. The other major source of systematic uncertainty is the closure of the background estimation methods, where closure refers to tests which demonstrate that the background determination techniques described above reproduce the expected background distributions in both rate and shape to within the statistical uncertainties. The closure systematic uncertainty varies from 2% to 6% percent for non-QCD multijet backgrounds. The systematic uncertainty resulting from the closure and normalization for the QCD multijet background is determined by the deviation of the tight-to-loose ratios obtained in the Z+jets region from those in the W+jets region. This uncertainty for the QCD multijet background depends on $p_T(\tau_h)$ and varies from $\sim$ 4% to $\sim$ 29%. Shape-based systematic uncertainties resulting from the use of the ISR correction factors are determined by varying these factors by $\pm 1\sigma$ and examining the resultant effects on the m_T distribution for Z+jets and W+jets events. This shape-based uncertainty is a few percent at low values of m_T and as much as 15% at high m_T values. Additional shape-based systematic uncertainties are assigned based on the level of agreement between

data and simulated m_{T} distributions in the control samples, where the predictions from simulation have been corrected using all the measured correction factors. The data/MC ratios of the m_{T} distributions are fit with a first-order polynomial, and the deviation of the fit from unity, as a function of m_{T}, is taken as the systematic uncertainty on the shape. This results in up to $\approx 20\%$ systematic uncertainty in a given m_{T} bin.

The efficiencies for the electron and muon reconstruction, identification, and isolation requirements are considered due to the extra lepton rejections in the SR and their use in the CRs. These efficiencies are measured with the "tag-and-probe" method with a resulting uncertainty of $\leq$ 1%, depending on the lepton p_{T} and η. The $p_{\mathrm{T}}^{\mathrm{miss}}$ scale uncertainties contribute via the jet energy scale (2-5% depending on η and p_{T}) and results in a systematic uncertainty of about 1-3% depending on m_T. A $p_{\mathrm{T}}^{\mathrm{miss}}$-dependent uncertainty in the measured trigger efficiency results in a 3% uncertainty in the signal and background predictions that rely on simulation.

The signal and minor backgrounds (estimated solely from simulation) are affected by similar sources of systematic uncertainty. The signal event acceptance for the ISR selection depends on the reconstruction and identification efficiency and energy scale of jets. The uncertainty in the signal acceptance due to the PDF set used in simulation is evaluated in accordance with the PDF4LHC recommendations [46] by comparing the results obtained using the CTEQ6.6L, MSTW2008nnlo, and NNPDF20 PDF sets with those from the default PDF set (CTEQ6L1) [47–49].

Figure 1 shows the $m_{\mathrm{T}}(p_{\mathrm{T}}^{\mathrm{miss}}, \tau_{\mathrm{h}})$ distribution for events in the SR. The binning used in Fig. 1 has been optimized to achieve the best discovery potential, resulting in ten bins of 10 GeV width between m_{T} of 0 and 120 GeV, four bins of 20 GeV width between m_{T} of 120 GeV and 200 GeV, and the overflow bin of 300 GeV width for $m_{\mathrm{T}} > 200$ GeV. No significant excess above the background prediction is observed. Therefore, 95% confidence level (CL) upper limits are set on the SSM1 signal production cross sections as function of $m(\widetilde{\chi}_1^{\pm})$ for fixed $\Delta m(\widetilde{\chi}_1^{\pm}, \widetilde{\chi}_1^0) = 50$ GeV and $m(\widetilde{\tau}) = 0.5m(\widetilde{\chi}_1^{\pm}) + 0.5m(\widetilde{\chi}_1^0)$ (Fig. 2 left). Similarly, Fig. 2 right shows the observed 95% CL upper limits on the SSM2 signal production cross sections as a function of $m(\widetilde{\tau})$ and $\Delta m(\widetilde{\tau}, \widetilde{\chi}_1^0)$. The limits are estimated following the modified frequentist construction $\mathrm{CL_s}$ method [50–52]. Maximum likelihood fits are performed using the final $m_{\mathrm{T}}(p_{\mathrm{T}}^{\mathrm{miss}}, \tau_{\mathrm{h}})$ distribution. Systematic uncertainties are represented by nuisance parameters, assuming a log-normal prior for the uncertainties in the data-driven background estimations and simulation-driven normalization parameters, and Gaussian priors for the shape uncertainties. Statistical uncertainties in the shape templates are accounted for by the technique described in Ref. [53].

We exclude $\widetilde{\chi}_2^0/\widetilde{\chi}_1^{\pm}$ with masses below 290 GeV for $\Delta m(\widetilde{\chi}_1^{\pm}, \widetilde{\chi}_1^0) = 50$ GeV and $\Delta m(\widetilde{\chi}_1^{\pm}, \widetilde{\tau}) = 25$ GeV, with 77.2 fb^{-1} of 13 TeV data from the LHC. The experimental constraints on the SUSY parameters with $\Delta m(\widetilde{\chi}_1^{\pm}, \widetilde{\chi}_1^0) = 50$ GeV and $\Delta m(\widetilde{\chi}_1^{\pm}, \widetilde{\tau}) = 25$ GeV using non-ISR searches have not exceeded those of the LEP experiments [24–27], and thus this new search complements the current analyses performed by the CMS and ATLAS collaborations.

In summary, we have presented a search for compressed supersymmetry in the stau-neutralino ($\tilde{\tau} - \widetilde{\chi}_1^0$) coannihilation region. It is the first collider search with exactly one soft, hadronically-decaying tau (τ) lepton and a large transverse momentum imbalance ($p_{\mathrm{T}}^{\mathrm{miss}}$) resulting from the recoil effect of high transverse momentum jet from initial state radiation (ISR). The search utilizes data corresponding to an integrated luminosity of 77.2 fb^{-1} collected in 2016 and 2017 with the CMS detector in proton-proton collisions at $\sqrt{s} = 13$ TeV. This particular search targets compressed mass spectra where the mass difference between the chargino ($\widetilde{\chi}_1^{\pm}$), or the next-to-lightest neutralino ($\widetilde{\chi}_2^0$), and the neutralino ($\widetilde{\chi}_1^0$), denoted by (Δm), is 50 GeV. This is motivated by models considering $\widetilde{\tau}$-$\widetilde{\chi}_1^0$ co-annihilation aiming to maintain consistency in the estimation

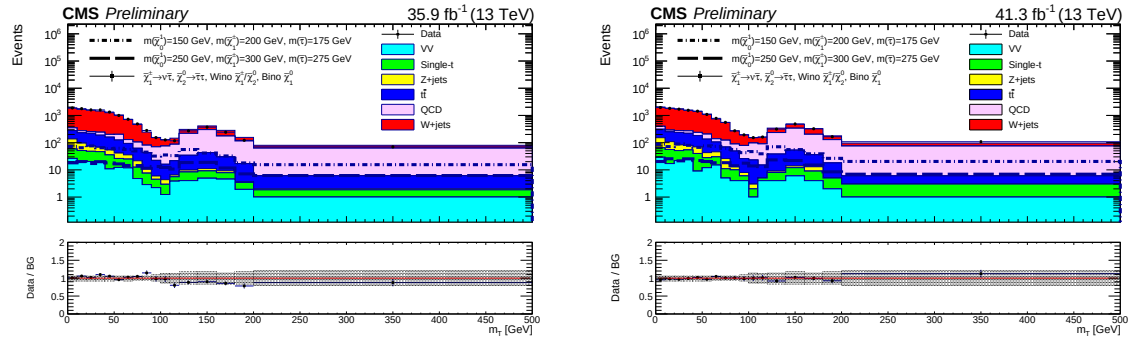

Figure 1: The $m_{\mathrm{T}}(p_{\mathrm{T}}^{\mathrm{miss}}, \tau_{\mathrm{h}})$ distribution for SR events with 2016 data (left) and 2017 data (right). On the top canvas of the figures, the solid colors correspond to the expected background processes, the black dots to the observed data, and the dashed lines to the expected signal from simulation. The bottom canvas of the figures show the ratio between the observed data and the total expected background. The shaded band correspond to the total statistical uncertainty.

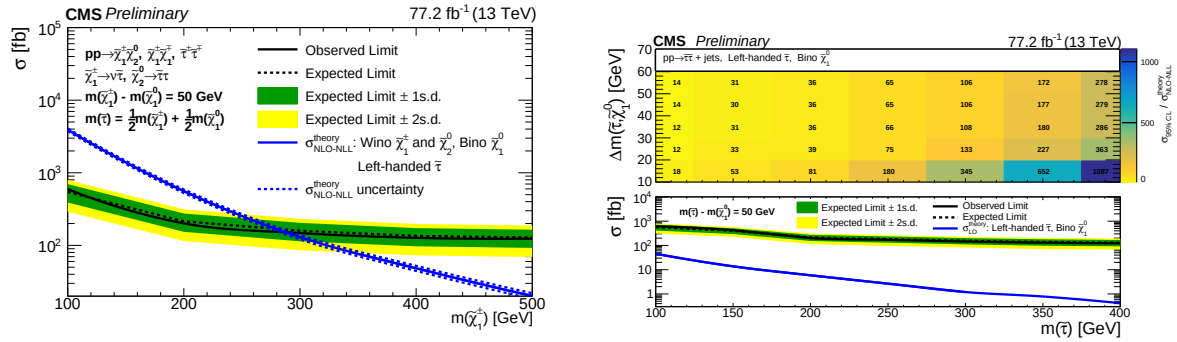

Figure 2: The plot on the left shows the 95% confidence level (CL) upper limits on the $\widetilde{\chi}_1^{\pm}$ and $\widetilde{\chi}_2^0$ pair production cross sections in SSM1, as function of $m(\widetilde{\chi}_1^{\pm})$. The solid blue line corresponds to the theoretical cross section. The observed limit is shown with the solid black line, while the expected limit is represented with the dashed black line. The yellow (green) band corresponds to the one (two) standard deviation from the central value of the expected limit. The plot on the right, top canvas, presents the ratio of the 95% CL upper limit on the direct $\widetilde{\tau}$ pair production signal cross section in SSM2 to the theoretical cross section, as function of $m(\widetilde{\tau})$ and $\Delta m(\widetilde{\tau}, \tilde{\chi}_1^0)$. The bottom canvas presents the 95% CL upper limits on the direct $\tilde{\tau}$ pair production signal cross sections in SSM2, as function of $m(\widetilde{\tau})$ for $m(\widetilde{\tau}) - m(\tilde{\chi}_1^0) = 50\,\mathrm{GeV}$. The extremely small $\widetilde{\tau}\widetilde{\tau}$ production cross sections make these SSM2 scenarios very challenging, especially when $\Delta m(\widetilde{\tau}, \tilde{\chi}_1^0) < 50\,\mathrm{GeV}$. For a $\widetilde{\tau}$ mass of 100 GeV, the observed limit is about 10 times the theoretical cross section.

of the relic dark matter density between particle physics and cosmology. In the context of the minimal supersymmetric standard model (MSSM), the search considers purely electroweak production of $\widetilde{\tau}$s via cascading decays of $\tilde{\chi}_1^{\pm}$s and $\tilde{\chi}_2^0$s as well as direct production of $\widetilde{\tau}$s. The data do not reveal any evidence for new physics. The results are used to exclude a range of $\tilde{\chi}_1^{\pm}$ masses for a mass splitting $\Delta m(\tilde{\chi}_1^{\pm}, \tilde{\chi}_1^0)$ of 50 GeV. For $\Delta m(\tilde{\chi}_1^{\pm}, \tilde{\chi}_1^0) = 50\,\mathrm{GeV}$ and $Br(\tilde{\chi}_1^{\pm} \to \tilde{\tau}\nu \to \tau\tilde{\chi}_1^0\nu) = 100\%$, $\tilde{\chi}_1^{\pm}$ masses up to 290 GeV are excluded at 95% CL. This sensitivity exceeds that of other $\tilde{\tau}$ searches to date [20–23].

References

[1] P. Ramond, "Dual theory for free fermions", *Phys. Rev. D* **3** (1971) 2415, doi:10.1103/PhysRevD.3.2415.

[2] Y. A. Gol'fand and E. P. Likhtman, "Extension of the algebra of Poincare group generators and violation of P invariance", *JETP Lett.* **13** (1971) 323.

[3] S. Ferrara and B. Zumino, "Supergauge invariant Yang-Mills theories", *Nucl. Phys. B* **79** (1974) 413, doi:10.1016/0550-3213(74)90559-8.

[4] J. Wess and B. Zumino, "Supergauge transformations in four dimensions", *Nucl. Phys. B* **70** (1974) 39, doi:10.1016/0550-3213(74)90355-1.

[5] A. H. Chamseddine, R. Arnowitt, and P. Nath, "Locally Supersymmetric Grand Unification", *Phys. Rev. Lett.* **49** (1982) 970, doi:10.1103/PhysRevLett.49.970.

[6] R. Barbieri, S. Ferrara, and C. A. Savoy, "Gauge models with spontaneously broken local supersymmetry", *Phys. Lett. B* **119** (1982) 343, doi:10.1016/0370-2693(82)90685-2.

[7] L. Hall, J. Lykken, and S. Weinberg, "Supergravity as the messenger of supersymmetry breaking", *Phys. Rev. D* **27** (1983) 2359, doi:10.1103/PhysRevD.27.2359.

[8] S. Dimopoulos and G. F. Giudice, "Naturalness constraints in supersymmetric theories with nonuniversal soft terms", *Phys. Lett. B* **357** (1995) 573, doi:10.1016/0370-2693(95)00961-J, arXiv:hep-ph/9507282.

[9] WMAP Collaboration, "First year Wilkinson Microwave Anisotropy Probe (WMAP) observations: Determination of cosmological parameters", *Astrophys. J. Suppl.* **148** (2003) 175–194, doi:10.1086/377226, arXiv:astro-ph/0302209.

[10] Planck Collaboration, "Planck 2015 results. XIII. Cosmological parameters", *Astron. Astrophys.* **594** (2016) A13, doi:10.1051/0004-6361/201525830, arXiv:1502.01589.

[11] R. L. Arnowitt et al., "Detection of SUSY signals in stau neutralino co-annihilation region at the LHC", *AIP Conf. Proc.* **903** (2007) 229, doi:10.1063/1.2735167, arXiv:hep-ph/0611089.

[12] V. Khotilovich, R. L. Arnowitt, B. Dutta, and T. Kamon, "The Stau neutralino co-annihilation region at an international linear collider", *Phys. Lett. B* **618** (2005) 182, doi:10.1016/j.physletb.2005.04.078, arXiv:hep-ph/0503165.

[13] M. Carena et al., "Light Stau Phenomenology and the Higgs $\gamma\gamma$ Rate", *JHEP* **07** (2012) 175, doi:10.1007/JHEP07(2012)175, arXiv:1205.5842.

[14] A. Aboubrahim, P. Nath, and A. B. Spisak, "Stau coannihilation, compressed spectrum, and SUSY discovery potential at the LHC", *Phys. Rev. D* **95** (2017) 115030, doi:10.1103/PhysRevD.95.115030, arXiv:1704.04669.

[15] G. H. Duan et al., "Vacuum stability in stau-neutralino coannihilation in MSSM", *Phys. Lett. B* **788** (2019) 475, doi:10.1016/j.physletb.2018.12.001, arXiv:1809.10061.

[16] R. Arnowitt et al., "Determining the dark matter relic density in the minimal supergravity stau-neutralino coannihilation region at the large hadron collider", *Phys. Rev. Lett.* **100** (2008) 231802, doi:10.1103/PhysRevLett.100.231802, arXiv:hep-ph/08022968.

[17] B. Dutta et al., "Vector boson fusion processes as a probe of supersymmetric electroweak sectors at the LHC", *Phys. Rev. D* **87** (2013) 035029, doi:10.1103/PhysRevD.87.035029, arXiv:1210.0964.

[18] A. G. Delannoy et al., "Probing Dark Matter at the LHC Using Vector Boson Fusion Processes", *Phys. Rev. Lett.* **111** (2013) 061801, doi:10.1103/PhysRevLett.111.061801, arXiv:1304.7779.

[19] A. Florez et al., "Probing the Stau-Neutralino Coannihilation Region at the LHC with a soft tau lepton and an ISR jet", *Phys. Rev. D* **94** (2016) 073007, doi:10.1103/PhysRevD.94.073007, arXiv:hep-ph/160608878.

[20] CMS Collaboration, "Combined search for electroweak production of charginos and neutralinos in proton-proton collisions at $\sqrt{s} = 13$ TeV", *JHEP* **03** (2018) 160, doi:10.1007/JHEP03(2018)160, arXiv:1801.03957.

[21] CMS Collaboration, "Search for new physics in events with two soft oppositely charged leptons and missing transverse momentum in proton-proton collisions at $\sqrt{s} = 13$ TeV", *Phys. Lett. B* **782** (2018) 440, doi:10.1016/j.physletb.2018.05.062, arXiv:1801.01846.

[22] ATLAS Collaboration, "Search for the direct production of charginos and neutralinos in final states with tau leptons in $\sqrt{s} = 13$ TeV pp collisions with the ATLAS detector", *Eur. Phys. J. C* **78** (2018) 154, doi:10.1140/epjc/s10052-018-5583-9, arXiv:1708.07875.

[23] ATLAS Collaboration, "Search for electroweak production of supersymmetric states in scenarios with compressed mass spectra at $\sqrt{s} = 13$ TeV with the ATLAS detector", *Phys. Rev. D* **97** (2017) 052010, doi:10.1103/PhysRevD.97.052010, arXiv:1712.08119.

[24] ALEPH Collaboration, "Search for scalar leptons in e+ e- collisions at center-of-mass energies up to 209-GeV", *Phys. Lett. B* **526** (2002) 206, doi:10.1016/S0370-2693(01)01494-0, arXiv:hep-ex/0112011.

[25] DELPHI Collaboration, "Searches for supersymmetric particles in e+ e- collisions up to 208-GeV and interpretation of the results within the MSSM", *Eur. Phys. J. C* **31** (2003) 421, doi:10.1140/epjc/s2003-01355-5, arXiv:hep-ex/0311019.

[26] L3 Collaboration, "Search for scalar leptons and scalar quarks at LEP", *Phys. Lett. B* **580** (2004) 37, doi:10.1016/j.physletb.2003.10.010, arXiv:hep-ex/0310007.

[27] OPAL Collaboration, "Search for anomalous production of dilepton events with missing transverse momentum in e+ e- collisions at $\sqrt{s}$ = 183-Gev to 209-GeV", *Eur. Phys. J. C* **32** (2004) 453, doi:10.1140/epjc/s2003-01466-y, arXiv:hep-ex/0309014.

[28] CMS Collaboration, "The CMS experiment at the CERN LHC", *JINST* **3** (2008) S08004, doi:10.1088/1748-0221/3/08/S08004.

[29] CMS Collaboration, "Particle-flow reconstruction and global event description with the cms detector", *JINST* **12** (2017) P10003, doi:10.1088/1748-0221/12/10/P10003, arXiv:1706.04965.

[30] M. Cacciari, G. P. Salam, and G. Soyez, "The anti-k_T jet clustering algorithm", *JHEP* **04** (2008) 063, doi:10.1088/1126-6708/2008/04/063, arXiv:0802.1189.

[31] CMS Collaboration, "Jet algorithms performance in 13 TeV data", CMS Physics Analysis Summary CMS-PAS-JME-16-003, 2016.

[32] CMS Collaboration, "Jet energy scale and resolution in the CMS experiment in pp collisions at 8 TeV", *JINST* **12** (2017) P02014, doi:10.1088/1748-0221/12/02/P02014, arXiv:1607.03663.

[33] CMS Collaboration, "Identification of heavy-flavour jets with the CMS detector in pp collisions at 13 TeV", *JINST* **13** (2018) P05011, doi:10.1088/1748-0221/13/05/P05011, arXiv:1712.07158.

[34] CMS Collaboration, "Performance of electron reconstruction and selection with the CMS detector in proton-proton collisions at $\sqrt{s} = 8$ TeV", *JINST* **10** (2015) P06005, doi:10.1088/1748-0221/10/06/P06005, arXiv:1502.02701.

[35] CMS Collaboration, "Performance of the CMS muon detector and muon reconstruction with proton-proton collisions at $\sqrt{s} = 13$ TeV", *JINST* **13** (2018) P06015, doi:10.1088/1748-0221/13/06/P06015, arXiv:1804.04528.

[36] CMS Collaboration, "Performance of reconstruction and identification of τ leptons decaying to hadrons and ν_τ in pp collisions at $\sqrt{s} = 13$ TeV", *JINST* **13** (2018) P10005, doi:10.1088/1748-0221/13/10/P10005, arXiv:1809.02816.

[37] J. Alwall et al., "The automated computation of tree-level and next-to-leading order differential cross sections, and their matching to parton shower simulations", *JHEP* **07** (2014) 079, doi:10.1007/JHEP07(2014)079, arXiv:1405.0301.

[38] T. Sjöstrand et al., "An introduction to PYTHIA 8.2", *Comput. Phys. Commun.* **191** (2015) 159, doi:10.1016/j.cpc.2015.01.024, arXiv:1410.3012.

[39] CMS Collaboration, "Event generator tunes obtained from underlying event and multiparton scattering measurements", *Eur. Phys. J. C* **76** (2016) 155, doi:10.1140/epjc/s10052-016-3988-x, arXiv:1512.00815.

[40] GEANT4 Collaboration, "GEANT4: A Simulation toolkit", *Nucl. Instrum. Meth.* **A506** (2003) 250–303, doi:10.1016/S0168-9002(03)01368-8.

[41] CMS Collaboration, "The fast simulation of the CMS detector at LHC", *J. Phys. Conf. Ser.* **331** (2011) 032049, doi:10.1088/1742-6596/331/3/032049.

[42] J. Debove, B. Fuks, and M. Klasen, "Threshold resummation for gaugino pair production at hadron colliders", *Nucl. Phys. B* **842** (2011) 51–85, doi:10.1016/j.nuclphysb.2010.08.016, arXiv:1005.2909.

[43] B. Fuks, M. Klasen, D. R. Lamprea, and M. Rothering, "Gaugino production in proton-proton collisions at a center-of-mass energy of 8 TeV", *JHEP* **10** (2012) 081, doi:10.1007/JHEP10(2012)081, arXiv:1207.2159.

[44] B. Fuks, M. Klasen, D. R. Lamprea, and M. Rothering, "Precision predictions for electroweak superpartner production at hadron colliders with RESUMMINO", *Eur. Phys. J. C* **73** (2013) 2480, doi:10.1140/epjc/s10052-013-2480-0, arXiv:1304.0790.

[45] J. Fiaschi and M. Klasen, "Neutralino-chargino pair production at NLO+NLL with resummation-improved parton density functions for LHC Run II", *Phys. Rev. D* **98** (2018), no. 5, 055014, doi:10.1103/PhysRevD.98.055014, arXiv:1805.11322.

[46] J. Butterworth et al., "PDF4LHC recommendations for LHC run II", *J. Phys. G* **43** (2016) 023001, doi:10.1088/0954-3899/43/2/023001, arXiv:1510.03865.

[47] P. M. Nadolsky et al., "Implications of CTEQ global analysis for collider observables", *Phys. Rev. D* **78** (2008) 013004, doi:10.1103/PhysRevD.78.013004, arXiv:0802.0007.

[48] A. D. Martin, W. J. Stirling, R. S. Thorne, and G. Watt, "Update of parton distributions at NNLO", *Phys. Lett. B* **652** (2007) 292, doi:10.1016/j.physletb.2007.07.040, arXiv:0706.0459.

[49] M. Ubiali, "NNPDF1.0 parton set for the LHC", *Nucl. Phys. Proc. Suppl.* **186** (2009) 62, doi:10.1016/j.nuclphysbps.2008.12.020, arXiv:0809.3716.

[50] T. Junk, "Confidence level computation for combining searches with small statistics", *Nucl. Instrum. Meth. A* **434** (1999) 435, doi:10.1016/S0168-9002(99)00498-2, arXiv:hep-ex/9902006.

[51] A. L. Read, "Presentation of search results: the CL_s technique", *J. Phys. G* **28** (2002) 2693, doi:10.1088/0954-3899/28/10/313.

[52] ATLAS and CMS Collaborations, "Procedure for the LHC Higgs boson search combination in Summer 2011", Technical Report CMS-NOTE-2011-005, ATL-PHYS-PUB-2011-11, 2011.

[53] R. J. Barlow and C. Beeston, "Fitting using finite Monte Carlo samples", *Comput. Phys. Commun.* **77** (1993) 219, doi:10.1016/0010-4655(93)90005-W.